land

MDPI

Article

Quantitative Estimation of Saline-Soil Amelioration Using Remote-Sensing Indices in Arid Land for Better Management

Hesham M. Aboelsoud [1], Mohamed A. E. AbdelRahman [2,*], Ahmed M. S. Kheir [1,3], Mona S. M. Eid [1], Khalil A. Ammar [3], Tamer H. Khalifa [1] and Antonio Scopa [4]

[1] Soil, Water and Environment Research Institute (SWERI), Agricultural Research Centre (ARC), Giza 12112, Egypt; hm_aboelsoud@yahoo.com (H.M.A.); ahmed.kheir@arc.sci.eg (A.M.S.K.); mona.sobhy28@yahoo.com (M.S.M.E.); Tamer.khalifa@arc.sci.eg (T.H.K.)
[2] Division of Environmental Studies and Land Use, National Authority for Remote Sensing and Space Sciences (NARSS), Cairo 11769, Egypt
[3] International Center for Biosaline Agriculture, Dubai 14660, United Arab Emirates; kaa@biosaline.org.ae
[4] Scuola di Scienze Agrarie, Forestali, Alimentari ed Ambientali (SAFE), Università degli Studi della Basilicata, Viale dell'Ateneo Lucano 10, 85100 Potenza, Italy; antonio.scopa@unibas.it
* Correspondence: maekaoud@narss.sci.eg; Tel.: +20-100-478-1114

Abstract: Soil salinity and sodicity are significant issues worldwide. In particular, they represent the most dominant types of degraded lands, especially in arid and semi-arid regions with minimal rainfall. Furthermore, in these areas, human activities mainly contribute to increasing the degree of soil salinity, especially in dry areas. This study developed a model for mapping soil salinity and sodicity using remote sensing and geographic information systems (GIS). It also provided salinity management techniques (leaching and gypsum requirements) to ameliorate soil and improve crop productivity. The model results showed a high correlation between the soil electrical conductivity (ECe) and remote-sensing spectral indices SI_A, SI3, VSSI, and SI9 (R^2 = 0.90, 0.89, 0.87, and 0.83), respectively. In contrast, it showed a low correlation between ECe and SI5 (R^2 = 0.21). The salt-affected soils in the study area cover about 56% of cultivated land, of which the spatial distribution of different soil salinity levels ranged from low soil salinity of 44% of the salinized cultivated land, moderate soil salinity of 27% of salinized cultivated land, high soil salinity of 29% of the salinized cultivated land, and extreme soil salinity of 1% of the salinized cultivated land. The leaching water requirement (LR) depths ranged from 0.1 to 0.30 m ha^{-1}, while the gypsum requirement (GR) ranged from 0.1 to 9 ton ha^{-1}.

Keywords: soil salinity; sodicity; GIS; RS; leaching and gypsum requirement

Citation: Aboelsoud, H.M.; AbdelRahman, M.A.E.; Kheir, A.M.S.; Eid, M.S.M.; Ammar, K.A.; Khalifa, T.H.; Scopa, A. Quantitative Estimation of Saline-Soil Amelioration Using Remote Sensing Indices in Arid Land for Better Management. *Land* **2022**, *11*, 1041. https://doi.org/10.3390/land11071041

Academic Editors: Jinyan Zhan, Xinqi Zheng, Shaikh Shamim Hasan and Wei Cheng

Received: 31 May 2022
Accepted: 6 July 2022
Published: 8 July 2022

1. Introduction

Land degradation is one of the world's most severe environmental and socio-economic issues [1–3], occurring due to natural phenomena and anthropogenic factors that negatively impact land's ability to function effectively in an ecosystem which causes enormous challenges in achieving sustainable development goals [4–7]. Degraded lands could reach one-fifth of the total land in some countries [8,9]. Currently, salt-affected soil covers approximately 1.125 billion hectares, with anthropogenic activities affecting 76 million hectares. Soil salinity is a primary challenge to global food security and environmental sustainability. As climate change accelerates, the problem may soon spread to unaffected areas [10]. The high salinity levels could cause adverse effects on soil characteristics and plant physiology [11,12].

There is an urgent need to increase the area of agricultural land to meet the increasing demand for food due to the rapid population growth [13–15]. Therefore, one of the effective ways to raise the efficiency of the agricultural unit is land reclamation processes

[16]. This helps in fixing one or more defects in the soils that hinder and/or reduce agriculture productivity [17]. However, the traditional methods for reclamation operations are costly in time and effort [16]; therefore, looking to modern technologies to help in these calculations has become an urgent necessity.

Remote sensing and geographical information systems (GIS) are promising tools for assessing land degradation [18–22]. These tools can generate relevant maps and reliable spatial information to support decision making [23–25]. The earliest successful attempts to use remote sensing for the detection of salt-affected soils were preceded by Mougenot et al. [26]. The remote sensing and GIS datasets provide accurate information on large areas. Some satellite 'images' are low in cost, and the remote-sensing assessment tasks can be carried out in a shorter time than conventional fieldwork assessments [27–30]. The assessment results can be used to adequately manage soil and crops [31–34]. Using Landsat images allows for assessing the soil salinity features. The Landsat images are the best to capture soil salinity extent with different salinity levels [35–41]. In Egypt, several studies have also been conducted to map soil salinity using remote sensing and GIS datasets and showed reliable soil salinity results [42–57].

The prevalence of saline/sodic soils depends on two types of factors, namely, climatic factors and geomorphologic factors. Saline lands are found in regions with a continental climate or where droughts prevail, which leads to increased evaporation and salt accumulation [58–60]. Saline/sodic soils also spread in the lands of lakes, rivers, and sedimentary valleys, and abound in dry and semi-arid areas with little rain and high temperatures. All conditions are identical in the study area where the evaporation process accelerates the formation of salts and their ascent to the surface of the soil through its capillary property [31,32,61,62]. Saline soils have higher salt concentrations than usual, whereas sodic soils have higher concentrations of Na^+ than usual. Saline soils cause a chemical drought while sodic soils, conversely, cause waterlogging in soils [33]. Leaching is a vital soil management technique applied to salt-affected soil by adding supplemental irrigation water to remove salts from the root zone layers [26–28]. Understanding the hydraulic properties of the soil, water mobility, and salt dynamics are essential to correctly conduct the required leaching [63–65], while adding gypsum ($CaSO_4 \times 2\ H_2O$) to salt-affected soil is one of the oldest amendment methods. This method promotes the efficient replacement of Na^+ by exchangeable Ca^{2+} leading to the improvement in the soil's physical–chemical and enzymatic properties [66–73].

In Egypt, salinity accumulation, sodicity, and waterlogging are the main form of land degradation. Soil salinity and sodicity seriously affect agriculture production, where saline/sodic soils occupy 46% of the total Nile Delta area [74]. Egypt's croplands are entirely irrigated due to the country's extremely low rainfall and high rates of evaporation. The primary cause of secondary soil salinization in Egypt is the extensive irrigation of agriculture in arid climate conditions [74,75]. Additionally, irrigation with contaminated water from the polluted drains led to increasing in some metals' concentration due to anthropogenic pollution through the spreading of contaminated dredged materials on agricultural fields [76]. The soil salinization problem in Egypt, caused by the reuse of irrigation drainage waters and limits on rice plantings due to the shortage of irrigation water, raises an urgent need for the agricultural productivity of the Nile Delta through, for instance, subsurface drainage in waterlogged lands, land leveling, and use of gypsum amendments [74]. Especially in Egypt, at least 20% of all irrigated areas are salt-affected, and other estimates put the figure as high as 50%. The northern part of the Nile Delta in Egypt contains a huge region of heavy clay soils with shallow open drainage, limited permeability, and low productivity.

In the North Delta region, particularly in Egypt's Kafr El-Sheikh Governorate, there is a serious lack of irrigation water supply. Farmlands at the end of irrigation canals must use available drainage water to compensate for the lack of source of water [76–79]. Therefore, this study aims to integrate remote sensing and GIS techniques to produce amelioration maps of leaching (LR) and gypsum (GR) requirements in the study area.

2. Materials and Methods

2.1. Description of the Studied Area

Location: The study area covers 373,191 km², representing 28.1% of the total area of the Delta region and about 0.35% of the total area of Egypt. It is located in the Kafr El-Sheikh Governorate in the northern part of Egypt's Nile Delta. The latitude ranges from 31°00′ and 31° 15′ in the east and 31°00′ and 31°37′ in the north, and an altitude of 9.14 m above sea level. It is bounded in the north by the Mediterranean Sea, the southern Gharbia Governorate, the eastern part of Dakahlia Governorate, and the western province of Bihaira. (Figure 1). In the north part of the area, Lake Burullus is located within the borders of the governorate with an area of 148,562 hectares. The lake is connected to the Mediterranean through the Burullus spur, which is 44m-wide.

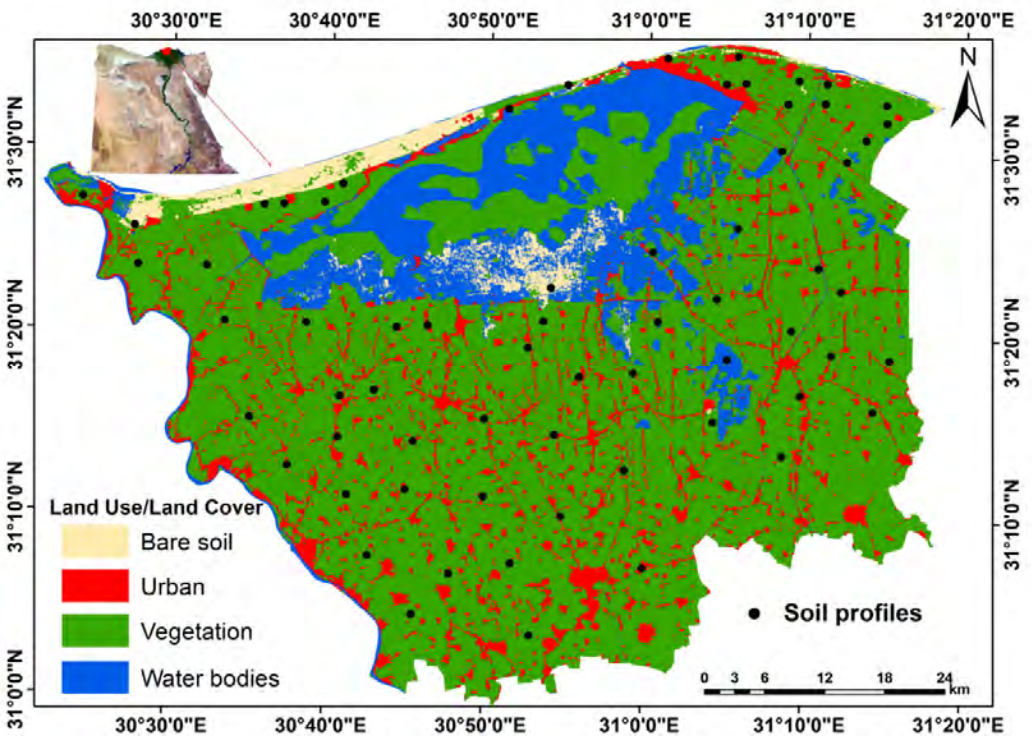

Figure 1. Location map of the study area.

Landform: The region's topography has a diversity of natural life due to the diversity of environments and the diversity of the topography of the land. The natural environments in the province can be classified into three main types: agricultural and urban environments, coastal environments, and wetlands. Each of them is unique in its animal life, plants, and biodiversity [80,81].

Geology: The center and south of the province cover the sediments of the modern geological age (Holocene era), which are dark-brown formations composed of deposits of clay, clay, and sandy clay. These sediments are deposited over the ancient marine sediments (under delta formations) that date back to the Pleistocene era. They are yellow in color and consist of coarse and fine sand and pebbles consisting of quartz or igneous and metamorphic rocks. The northern coastal zone is a low, sandy coast consisting of soft, brittle sediments belonging to the Pleistocene and Holocene [82,83].

All the ancient geological studies show that the Burullus region in the north of the governorate was less arid than our present era with the presence of many plants. Likewise, the shore of the delta region was mainly composed of silt, with swamps and depressions increasing in it. In the flood season, these depressions were filled with fresh water,

forming a series of small lakes and wetlands. These bogs were filled with organic matter and sediments resulting from the analysis of plant remains, so most of this water was devoid of oxygen. It was also filled with the shells of some bivalve mollusks, especially the cardium type. The coastal area consists of a sandy beach as a result of the sediments that were carried by the waves of the Mediterranean [82,83].

Climate: In general, the climate in Kafr el-Sheikh Governorate is an arid climate (classified as BWh) by the Köppen–Geiger system. The warmest month is August (31 °C), and the coldest month is January (9.4 °C). The total number of rainy days in a year is 31 days, where January is the wettest month while July is the driest month (0.0 mm/0 inches).

A climate diagram (Figure 2) is based on 30 years of available data from the study area. From this indication of typical climate patterns and conditions of temperature and precipitation, it is clear from the figure that the rain is very little, at less than 25 mm, and most of it occurs in January. Generally, the governorate has a Mediterranean climate, and the temperature varies between 13.2 °C in January (winter) and 26.6 °C in July (summer). The amount of precipitation ranges from 140 mm to 250 mm per year. The winds are generally western and northwest.

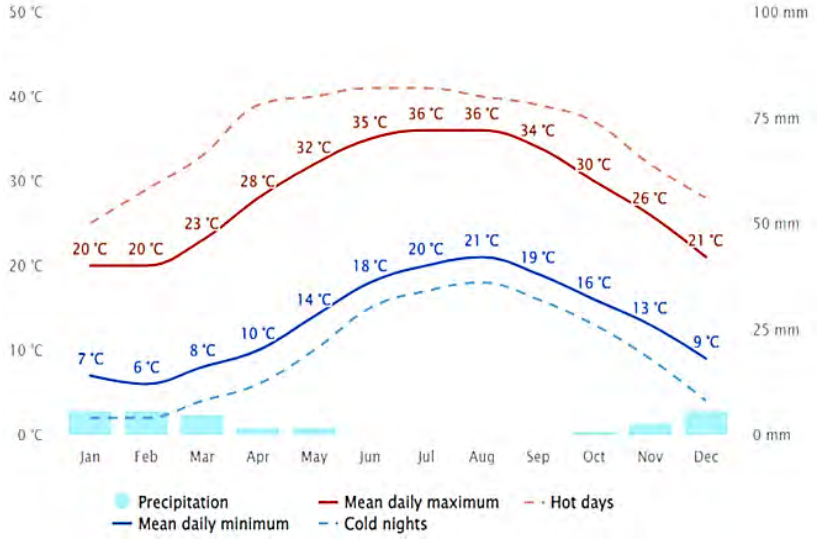

Figure 2. Climate parameters of the studied area.

Agricultural land and irrigation water: Soil texture in the study area is classified from heavy clay to sandy soil. Surface irrigation systems use the Nile water or drainage reuse, and it has electrical conductivity values between 0.31 and 1.86 dS m^{-1}.

The soil texture classes of the researched area differ between sandy and heavy clay, according to field surveys and laboratory investigations. Cation-exchangeable capacity (CEC) was strongly associated with clay content and ranged from 7.36 to 44.87 $cmol_c$ kg^{-1}. These soils ranged from being non-saline to being extremely salty according to the salinity levels, which ranged from 0.81 to 10.80 dS m^{-1}. ESP and pH values ranged from 1.02 to 36.20 and 7.83 to 8.81, respectively. The study area's bulk density and soil depth were between (1.11 and 1.63 Mg m^{-3}) and (120 to 150 cm), respectively. Organic matter generally is on average 16.2 g kg^{-1}. The high temperature in dry and semi-arid locations, which causes the decomposition of fresh residuals, is to blame for the low value of OM. $CaCO_3$ content is 7.30 g kg^{-1} on average.

The area of agricultural land in the governorate represents about 7.5% of the total agricultural area in Egypt [84–86]. Winter rains that fall on the northern coast of the area are unreliable. Groundwater cannot be used due to its excessive salinity as a result of seawater intrusion as well as to limit its effects. The efficiency of the applied surface irrigation system does not exceed 60% [84]. Recently, the governorate's share of fresh

water available for agriculture was about 3.15 billion cubic meters, and agricultural drainage water is mixed with freshwater canals to meet agricultural water requirements [85]. Drainage water with low-quality water such as wastewater is used for irrigation [86], especially in the areas located at the end of irrigation networks that receive inadequate fresh water. There are some main drains in the area such as West El-Burullus, Gharbia, El-Khashaah, Tirrah, and El-Hoks [87]. The principal pollutants are biological oxygen demand (BOD), chemical oxygen demand (COD), and NO_3-N. While NH_4-N and NO_3-N values fall within the normal range for irrigation, they are in the abnormal range according to Egyptian standards. BOD and COD values are rated as bad to moderate and moderate. According to Egyptian standards, the values are within the usual range for irrigation. Furthermore, except for Ni, whose readings are within the normal range, the levels of the heavy metals Cu, Mn, Pb, and Cd are higher than what is permitted for irrigation. B values in water samples range from poor to excellent. In the meantime, irrigation-appropriate pH values ranged from 7.33 to 8.15, EC values ranged from 1.87 to 4.71 ds m^{-1}, and SAR values ranged from 5.86 to 9.32.

2.2. Soil Analysis

Soil sampling was conducted in the study area, where 66 soil samples were collected at 0–0.3 m depths. The samples were dried, grounded, and passed through a 2.0 mm sieve in the laboratory (Table 1). The soil reaction (pH) and soil electrical conductivity (ECe, dS m^{-1}) were identified according to the Page method [87]. The soil organic matter (SOM, g kg^{-1}) was determined according to Nelson and Sommers method [88]. The Ca^{2+} as carbonate ($CaCO_3$, g kg^{-1}) was measured volumetrically using a Collins calcimeter method [89]. The exchangeable sodium percentage (ESP) was calculated using the [33] equation:

$$\mathrm{ESP} = \frac{100\times(-0.0126+0.01475\ \mathrm{SAR})}{1+(-0.0126+0.01475\ \mathrm{SAR})} \quad (1)$$

where SAR (sodium adsorption ratio) is a measure of the amount of sodium (Na^+) relative to calcium (Ca^{2+}) and magnesium (Mg^{2+}) in the water extracted from a saturated soil paste. It is the ratio of the Na concentration divided by the square root of one-half of the Ca + Mg concentration. SAR is calculated from the equation:

$$\mathrm{SAR} = Na^+/[(Ca^{2+} + Mg^{2+})/2]^{0.5}$$

Soils that have values for sodium adsorption ratio of 13 or more may have an increased dispersion of organic matter and clay particles, reduced saturated hydraulic conductivity and aeration, and a general degradation of soil structure.

Table 1. Basic variables for the sixty-six soil samples' studied soil properties.

Variable	Unit	Min	Max	Mean
pH (1:2.5 suspension)	-	7.83	8.81	8.32
ECe (paste extract)	dS m^{-1}	0.81	10.80	5.81
SAR	-	1.56	39.33	20.45
ESP	-	1.02	36.20	18.61
SOM	g kg^{-1}	10.5	21.9	16.2
$CaCO_3$	g kg^{-1}	0.33	14.27	7.30

2.3. Soil Amelioration

Leaching requirements (LR, depth cm) were calculated using the [90] equation:

$$\mathrm{LR} = \frac{\mathrm{EC_{iw}}}{5 \times (\mathrm{EC_e} - \mathrm{EC_{iw}})} \quad (2)$$

where EC_{iw} is the electrical conductivity of the irrigation water and EC_e is the soil electrical conductivity.

Gypsum requirements (GR, Mg ha^{-1}) were calculated using the [33] equation.

$$GR = \frac{ESP_i - ESP_f}{100} \times CEC \times 4.1 \quad (3)$$

where ESP_i: actual ESP of the soil; ESP_f: ESP required to be reached by reclamation; and CEC: cation exchange capacity ($cmol_c$ kg^{-1}).

2.4. Image Preprocessing and Analysis

2.4.1. Remote-Sensing Data

Remote sensing provides spatial coverage by measuring reflected and emitted electromagnetic radiation from the earth's surface and surrounding atmosphere over a wide range of wavelengths. Remote sensing implies collecting data without making physical contact with the studied object. This study used Landsat 8 (OLI) images (path 177, row 38) in May 2021.

2.4.2. Image Preprocessing

Image distortions and degradations occur during the acquisition process of remotely sensed images. Preprocessing satellite data are required to remove sensor errors during data acquisition and display the correction, band selection, data dimensionality reduction, and computing complexity reduction. The team conducted radiometric to eliminate radiometric problems in images such as nonuniformity, stripe noises, and defective lines, for proper conversion of digital numbers to reflectance values, geometric, and atmospheric corrections on the studied Landsat OLI images to increase the visual distinction between features.

2.4.3. Atmospheric Correction Using FLAASH Tool

The team conducted atmospheric correction using The FLAASH (fast line/of/sight atmospheric analysis of spectral hypercubes) tool in ENVI 5.1 software to have better reflectance. The team used the native file in a BSQ format for the correction and converted the images to BIL and BIP format to be compatible with the FLAASH tool.

2.5. Surface Interpolation Using the Ordinary Kriging Technique

The team used the interpolation method to determine the spatial variability and pattern of the soil characteristics in two-dimensional soil data sets in the topsoil. The geostatistical analyst extension (Arc GIS 10.4.1) [91] was used to develop the semi-variogram between each pair of points and interpolate between the sampling locations using the kriging method to predict the soil salinity in the study area. Ordinary kriging was used to estimate the value of continuous soil salinity (z) at an unsampled location (u) using only data on this characteristic [$z(u_\alpha)$, $\alpha = 1, n$] as a linear combination of neighboring observations:

$$Z^*_{ok}(U) = \sum_{\alpha=1}^{n(u)} \lambda_\alpha(u) Z(u_\alpha) \quad (4)$$

The ordinary kriging weights were chosen to minimize the estimation or error variance,

$$\sigma \frac{2}{E}(u) = Var[Z \quad (u) - Z(u)] \quad (5)$$

The weights were obtained by solving a system of linear equations:

$$\begin{cases} \sum_{\beta=1}^{n(u)} \lambda_\beta(u)\gamma(u_\alpha - u_\beta) - \mu(u) = \gamma(u_\alpha - u) \\ \sum_{\beta=1}^{n(u)} \lambda_\beta(u) = 1 \ \alpha = 1, \ldots, n\,(u) \end{cases} \quad (6)$$

To ensure the estimator was unbiased, constraining the weights to sum to one requires the definition of the Lagrange parameter m (u).

2.6. Soil Salinity Indices

The team examined fourteen different spectral salinity indices related to salt detection and soil salinity mapping developed in numerous studies. The most commonly used salinity indices taken into account in this study (NDSI, SI_A, SI 1, SI 2, SI 3, SI 4, SI 5, SI 6, SI 7, SI 8, SI 9, NDVI, SAVI, and VSSI) are presented in Table 2.

Table 2. Soil salinity indices based on different band ratios of Landsat.

No	Index Name	Formula	Ref.
1	Salinity index (SI)	$\sqrt{Band\ 3 \times Band\ 4}$	[92]
2	Soil salinity index for arid and semi-arid conditions (SI_A)	$SI_A = \frac{\left(\left(\frac{Blue \times Red}{Green}\right) \times \left(\frac{Red \times Near\ Infrared}{Green}\right)\right)}{\left(\frac{Blue - Red}{Blue + Red}\right)}$	[93]
3	Normalized difference salinity index (NDSI)	$\frac{Band\ 3 - Band\ 4}{Band\ 3 + Band\ 4}$	[94]
4	Vegetation soil salinity index (VSSI)	$2 \times Band2 - 5\ (Band\ 3 + Band\ 4)$	[92]
5	Normalized differential vegetation index (NDVI)	$\frac{Band4 - Band\ 3}{Band3 + Band\ 4}$	[94]
6	Soil adjusted vegetation index (SAVI)	$(1 + L)Band\ 4 - \left(\frac{Band\ 3}{L}\right) + Band\ 4 + Band\ 3$	[95]
7	Salinity index 2	$SI = \sqrt{G \times R}$	[92]
8	Salinity index 3	$SI = \sqrt{G^2 + R^2 + NIR^2}$	[96]
9	Salinity index 4	$SI = \sqrt{G^2 + R^2}$	[96]
10	Salinity index 5	$SI = \frac{B}{R}$	[97]
11	Salinity index 6	$SI = \frac{B - R}{B + R}$	[97]
12	Salinity index 7	$SI = \frac{B \times R}{B}$	[97]
13	Salinity index 8	$SI = \frac{B \times R}{G}$	[98]

Where: B, G, R, NIR, SWIR1, and SWIR2 refer to the reflectance in visible blue, green, red, near-infrared, Shortwave infrared 1, and 2, respectively.

The processing steps of mapping soil salinity using Landsat 8 image by the superior index among the used indices through assessing soil salinity from soil samples are shown in Figure 3. Firstly, FLAASH model was applied to remove the atmospheric effects [98–100]. Then, image processes were applied, i.e., image morphology, conversion from digital number to reflectance value, cloud filtering [101], and image enhancement. Subsequently, indices were computed and analyzed. Then, indices were normalized in Excel software. Secondly, the soil samples were analyzed with the spectral reflectance of the image. The soil salinity is estimated by the measured laboratory EC. Based on the results, the relationship was determined between reflectance values and indices of soil salinity to estimate the soil salinity from the image. It was noted that various soil types reflect solar radiation differently. The variation in reflectance makes it possible to identify the type of

soil at the surface layer. Validation samples were taken from different land use/land cover types, including Sabkha, water bodies, waterlogged, bare soil, and cultivated land. The sample locations are selected at different salinity intrusion degrees. Finally, leaching water requirements and Gypsum requirements were calculated as shown in Figure 3.

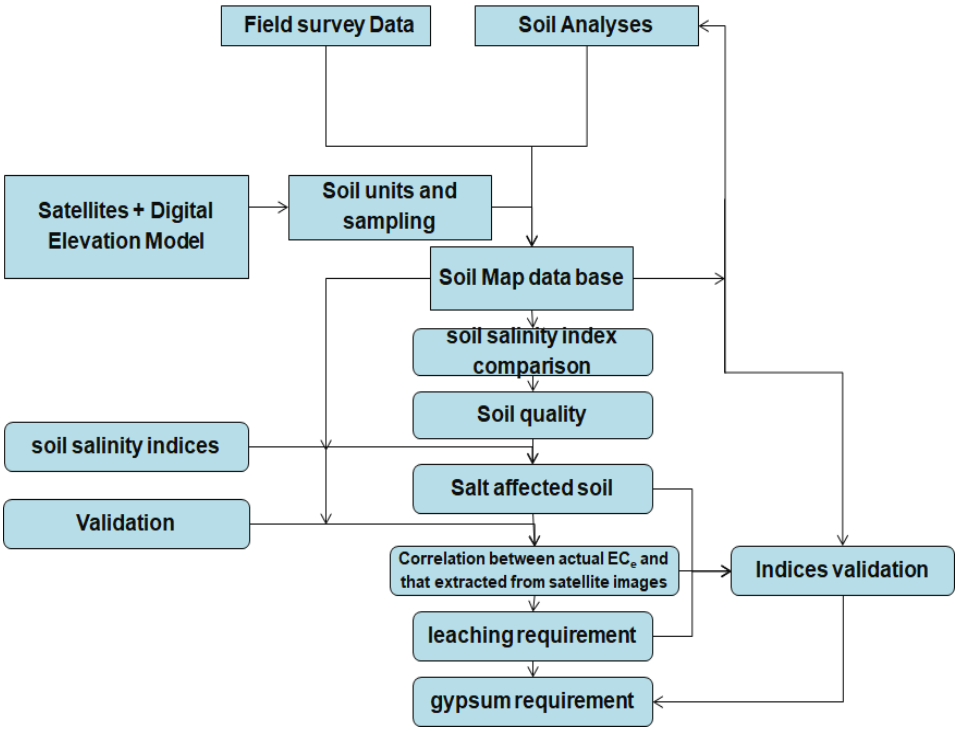

Figure 3. The workflow of saline soil amelioration using Landsat 8 OLI image.

3. Results

3.1. The Relationship between ECe and Remote-Sensing Spectral Indices

Various spectral indices derived from the initial Landsat bands in the study area validated the developed spatial model of soil salinity; Figure 4. The statistical correlation between soil electrical conductivity (ECe) and remote-sensing spectral index revealed that the salinity index (SI_A), salinity index 3 (SI3), vegetation soil salinity index (VSSI), and salinity index 9 (SI9) had a significant correlation with ECe (R^2 = 0.90, 0.89, 0.87, and 0.83, respectively). However, salinity index 5 (SI5) had a low correlation (R^2 = 0.21). The models with the highest R^2 values, indicating a high correlation between field measurement data and satellite data, were chosen as the best regression model to produce the soil salinity map of the study area. Overall, the brightness index with bands (R and NIR) of the image dated May 2021 had the highest correlation of 90%. Therefore, this obtained regression equation was used for soil mapping, while the density-slicing method was used to classify the different salinity levels, according to the different salinity classes. These salinity classes were defined using the international salinity thresholds.

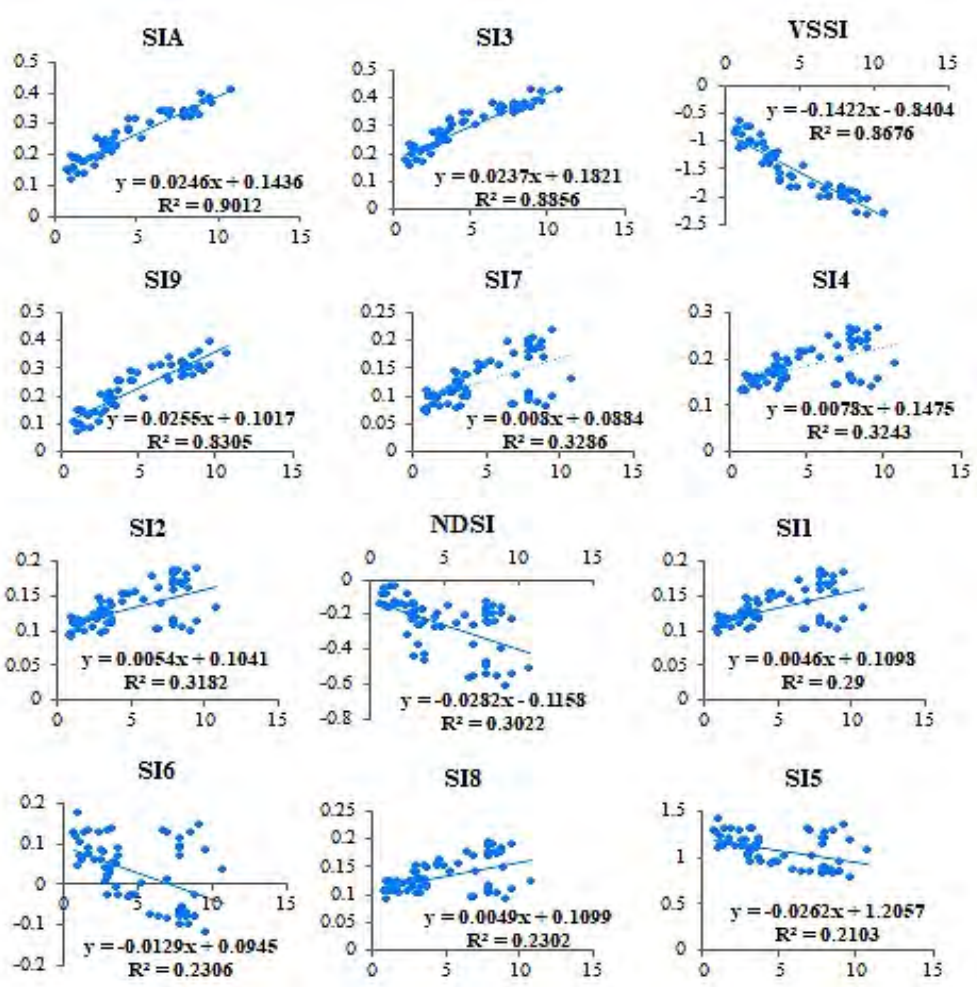
SIA
y = 0.0246x + 0.1436
R² = 0.9012
SI3
y = 0.0237x + 0.1821
R² = 0.8856
VSSI
y = -0.1422x - 0.8404
R² = 0.8676
SI9
y = 0.0255x + 0.1017
R² = 0.8305
SI7
y = 0.008x + 0.0884
R² = 0.3286
SI4
y = 0.0078x + 0.1475
R² = 0.3243
SI2
y = 0.0054x + 0.1041
R² = 0.3182
NDSI
y = -0.0282x - 0.1158
R² = 0.3022
SI1
y = 0.0046x + 0.1093
R² = 0.29
SI6
y = -0.0129x + 0.0945
R² = 0.2306
SI8
y = 0.0049x + 0.1099
R² = 0.2302
SI5
y = -0.0262x + 1.2057
R² = 0.2103

(**a**)

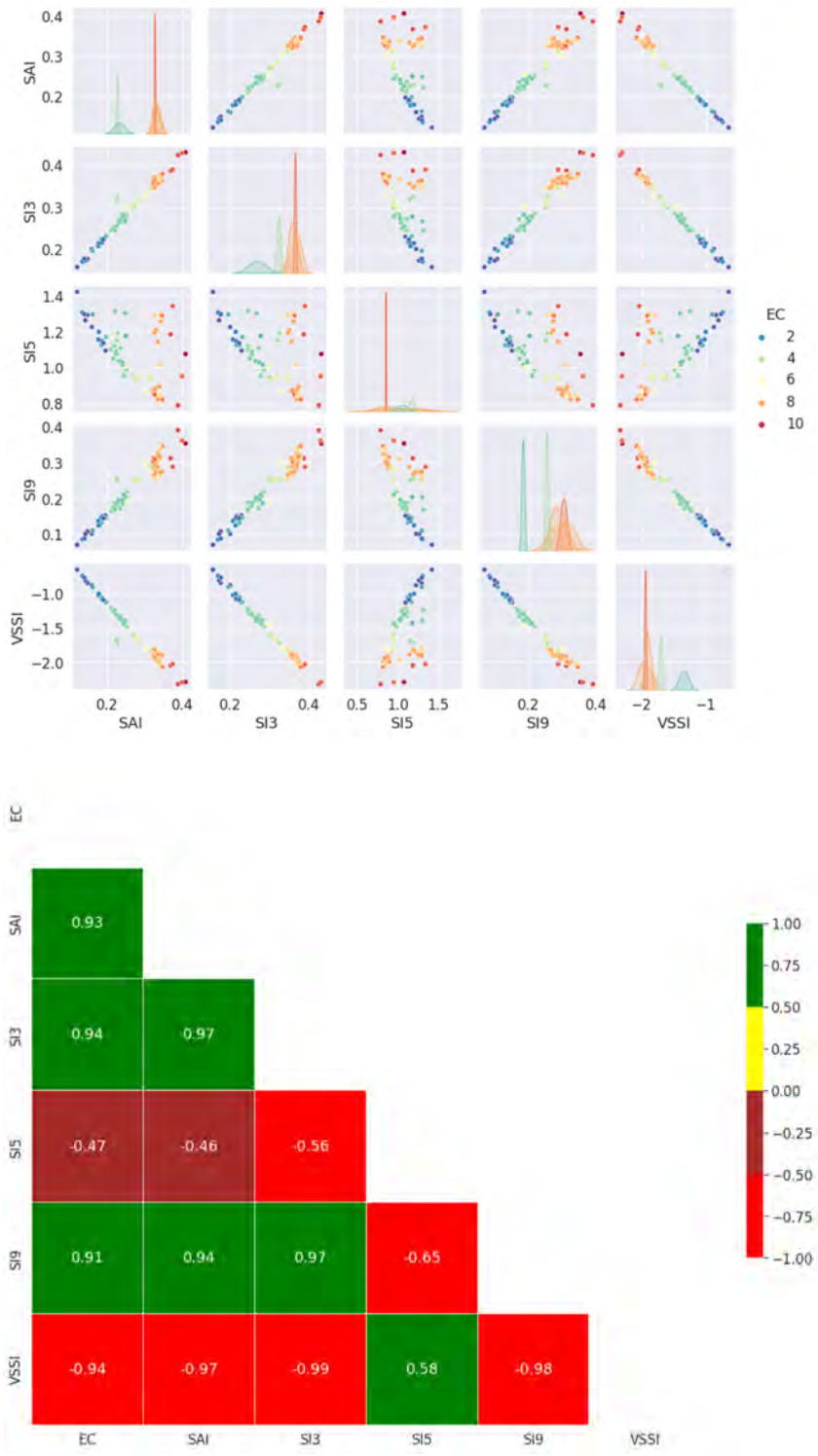

(**b**)

Figure 4. (**a**) The correlation between actual ECe and soil salinity indices. (**b**) The pair plot (**up**) and correlation (**down**) between the actual ECe and that extracted from satellite images.

The SI_A, SI2, SI3, SI4, SI7, SI8, and SI9 indices are positively correlated between the actual ECe and the modeled ECe, and negatively correlated with NDS1, SI6, and SI5. All

of the studied indicators followed a normal distribution for the low-salinity class (2 and 4 dS m^{-1}), while the higher-salinity class resulted in negative skewness. It was noted that there was a high level of uncertainty and variability for all indicators with higher salinity levels, but a lower level of uncertainty with lower salinity content (Figure 2).

3.2. Land Use

The land use in the study area was 373,191 ha and can be classified into four dominant classes: cultivated land, water bodies and lake Burrulus, fish ponds, and urban area. The cultivated land was the main class, the second class was water bodies and lake Burrulus, the third class was fish bonds, and the fourth class was the urban area, which covered about 72, 12, 10, and 6% of the total area, respectively (Table 3).

Table 3. The main land use categories in the study area.

Land Use Categories	Area (%)	Area (ha)
Cultivated land (C.A.)	72%	269,628
Water bodies and lake Burrulus	12%	43,512
Fish ponds	10%	37,739
Urban	6%	22,310
Total studied area	100%	373,189

3.3. Soil Quality Index (SQI)

The results related to classifying the different salinity levels by the salinity index SI_A with bands (R and NIR) are given in Table 4 and Figure 5. The results of the proposed model revealed that the assessment of salinity levels was classified into four classes: the low salinity (4 > dS m^{-1}) class occupies 118,580 ha (44% of the cultivated area); the moderate-salinity class (4–8 dS m^{-1}) occupies 73,177 ha (27% of the cultivated area); the high-salinity class (8–16 dS m^{-1}) represents 77 ha (28% of the cultivated area); and the extreme-salinity class (>16 dS m^{-1}) represents 145 ha (1% of the cultivated area). The results indicated that the salt-affected soils in the study area represent 56% of the cultivated land.

Table 4. The main salinity class categories in the study area.

Salinity Class (dS m^{-1})	Area ha	Area (%)
4>	118,580	44
4–8	73,177	27
8–16	77,726	28
16<	145	1
The cultivated study area	269,628	100%

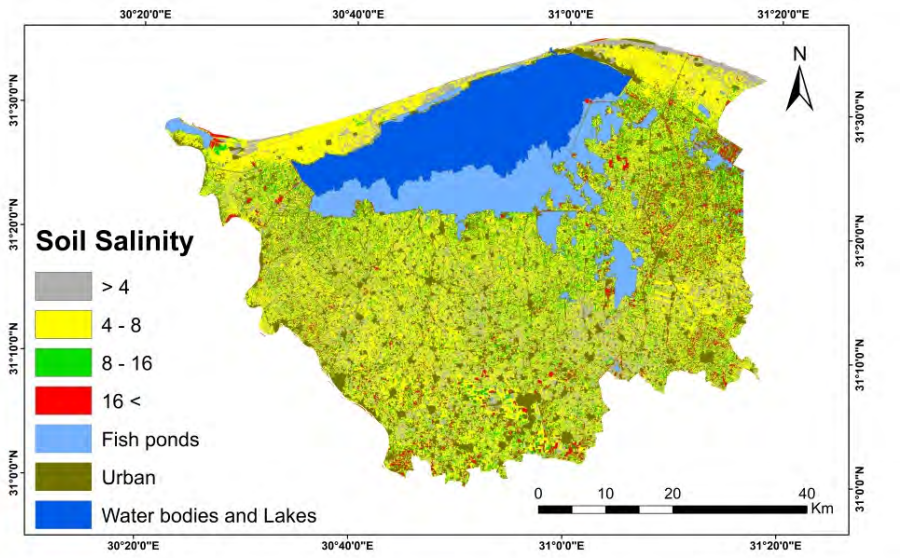

Figure 5. Results of soil salinity index for arid and semi-arid conditions (SIA) in the study area.

3.4. Soil Amelioration

3.4.1. Leaching Water Requirements

Figure 6 shows the different leaching requirements that should be added to the soil to reduce soil salinity. The different leaching water requirement depths were classified into six classes: (1) 0.01 to 0.1 m ha^{-1} for an area of about 27,607 ha (10% of the cultivated area); (2) 0.1 to 0.2 m ha^{-1} for an area of about 62,335 ha (23% of the cultivated area); (3) 0.2 to 0.3 m ha^{-1} for an area of about 66,775 ha (25% of the cultivated area); (4) 0.3 to 0.4 m ha^{-1} for an area of about 83,453 ha (31% of the cultivated area); (5) 0.4 to 0.6 m ha^{-1} for an area of about 15,447 ha (5% of the cultivated area); (6) 0.6 to 0.9 m water depth ha^{-1} for an area of about 14,012 ha (5% of the cultivated area).

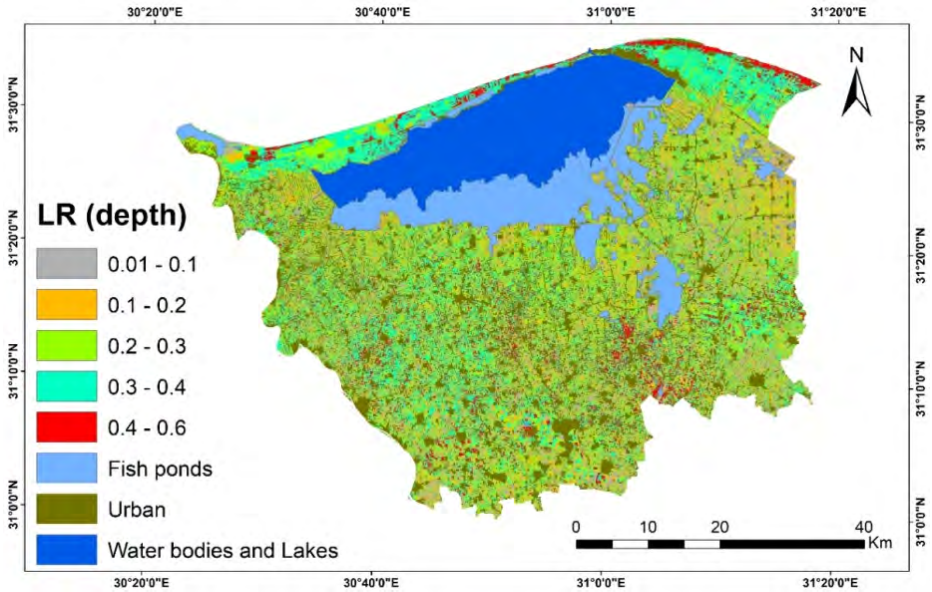

Figure 6. Different leaching requirements by satellite images for the study area.

3.4.2. Gypsum Requirements

Figure 7 illustrates the different gypsum requirements that should be added to the soil to reduce soil sodicity. As is clear from the figure, the gypsum requirement was classified into six classes: (1) 0.10 to 1 ton ha^{-1} for an area of 41,346 ha (15% of the cultivated area); (2) 1 to 2 ton ha^{-1} for an area of about 69,754 ha (26% of the cultivated area); (3) 2 to 3 ton ha^{-1} for an area of about 65,86 ha (24% of the cultivated area); (4) 3 to 4 ton ha^{-1} for an area of about 49,171 ha (18% of the cultivated area); (5) 4 to 6 ton ha^{-1} for an area of about 34,234 ha (13% of the cultivated area); (6) 6 to 9 ton ha^{-1} for an area of about 9265 ha (3% of the cultivated area).

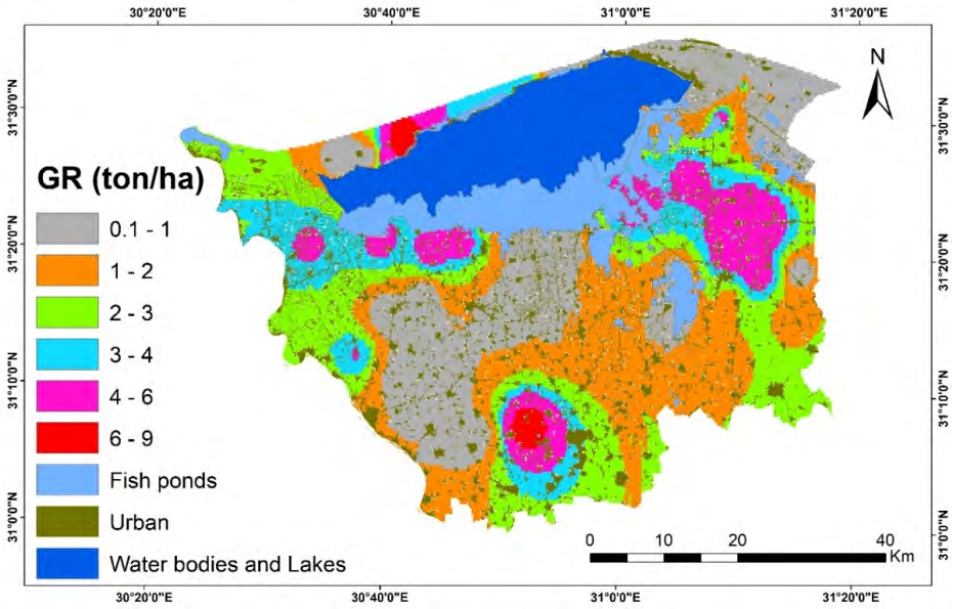

Figure 7. Different gypsum requirement assessments by GIS for the study area.

4. Discussion

Assessment of salt-affected soil using remote sensing and GIS is beneficial due to its low cost and efficiency. This will improve the management of the salt-affected soil [1]. It was clear from the results obtained that using Landsat images can capture soil salinity with a significant correlation between the ECe values and bands of the Landsat images [40–46].

Our results indicate that the correlation between the remote-sensing spectral index and ECe (salinity index (SI_A), salinity index 3, vegetation soil salinity index, and salinity index 9) was highly significant. This agrees with the views of [102,103] who emphasized that the salinity index (SI) has the highest correlation with soil salinity based on the image enhancement method. Elhag [104] indicated that the SI-3 and SI-9 have a high correlation with soil salinity indices.

The results showed that the salt-affected soils in the study area represent 56% of cultivated land. These results agree with one study [80,93], which stated that more than 50% of the soil in Kafr El-Sheikh Governorate suffers from land degradation. Additionally, good or non-saline soils in the study area decreased by 33% during the period 1961 to 2016 [81]. Another study conducted by Enar [105] indicated that the low-salinity soil increased by 0.46%, while moderate salinity, high salinity, and extreme soil salinity increased by 16%, 52%, and 20% during the period 2000 to 2020, respectively.

The added value of the paper is in mapping the soil water leaching and gypsum requirements using remote-sensing and GIS techniques. Limited studies have covered this topic so far. The method used to calculate the leaching water requirements (cm, depth)

and gypsum requirements (GR, Mg ha^{-1}) according to the concentration of salts is reliable and accurate [33,90]. The leaching water depths required to reduce the ECe ranged between 0.01 and 0.90 m ha^{-1}, while the gypsum required to reduce the initial ESP in different study zones ranged from 0.1 to 9 tons ha^{-1}.

The investigated salt-affected soils are formed as a result of climate and inappropriate soil management. This is in addition to the effect of irrigation water, water logging, and saline water intrusion of the Mediterranean. Saline, saline–sodic, and sodic soils have a strong presence in the area with an average of 55% of the total cultivated soils (Table 2). The south part of the area is threatened by sodicity according to the low-salinity soils and highly carbonated irrigation water, while the north of the area contains the highest area of saline and saline–sodic soils, reaching 33%. Poor drainage in addition to reuse of saline drainage water supports the buildup of salinity and sodicity [106]

The most popular method for reclaiming salt-affected soils in the region is a gypsum amendment ($CaSO_4$ 2 H_2O) combined with intermittent leaching. Another two ways for adapting and mitigating salinity and sodicity accumulation in the region are furrow irrigation and rice production under ponding.

The salts are spread in the soil profile, especially in the northern areas of the study area, adjacent to the water-logged areas, Sabkha, and along the coastline. The dominant salts in the delta are saline, and sodic soils are sodium sulfate (Na_2SO_4) and sodium carbonate and bicarbonate (Na_2CO_3 and $NaHCO_3$). The solubility of these salts decreases sharply with temperature decreases; accordingly, the reclamation and leaching processes should be applied during the summer warm season only. Improving drainage and preventing industrial and sanitary wastes in the agricultural drain is a must [107]. Land degradation in coastal areas, increased distribution of soil salinity, and reduced crop productivity in the region are the manifestations of climate change that have already appeared in the region from rising sea levels, coastal erosion, reduced Nile flow, increased summer temperature, changing rainfall patterns [108–112], and increased evapotranspiration [113].

In the study case, saline soils should be treated, and subsequently sodic soils, in order to reduce the concentration of salts to the appropriate degree for the growth of plant roots and even the appropriate depth for the roots [114–120].

Proper agricultural practices should be followed such as: adding organic fertilizers, developing and maintaining drainage, following an appropriate agricultural cycle, using a digger plow, and choosing salt-tolerant crops and an appropriate irrigation system.

Nitrate, phosphate, and potassium fertilization increase the resistance of plants to salinity. Salt-tolerant crops such as barley and sorghum are the most salt-resistant cereal crops, followed by rice and wheat, while maize is the least resistant. Cotton and sugar beet are the most important salt-tolerant crops, while sugar cane, fava beans, and peas are the least tolerant of salinity. Most vegetable crops are moderately resistant to salinity, while most fruit crops, especially deciduous, are sensitive to salinity [114–124].

5. Conclusions

The physico-chemical characteristics of 60 soil profiles were investigated. The results showed remarkable differences among various sites. The differences were very clear between the southern regions, where they are often affected by a slight or medium degree of deterioration and are often concentrated in soil compaction, while the northern regions were greatly degraded due to the presence of most types of soil deterioration such as salinity, alkaline, and waterlogging. The GIS, Landsat OLI satellite images, and multi-temporal satellite image analysis were used to estimate the rate and extent of salinized areas. These proven tools are handy for providing accurate and timely geospatial information depicting soil conditions. The results reflected that 56% of cultivated land of the Kafr El-Sheikh Governorate suffers from salinization. Zoning or classifying the area into zones can lead to better management and amelioration of the different salinity zones. Therefore, using this technology improves the management of salt-affected soil on a large

scale and can be regarded as one of the best management strategies for increasing crop production. The causes of salinity in investigated soils are thought to be a result of seawater intrusion—especially in the coastal zone of the area—high water table level, accumulation of salt in the upper soil layers due to unsuitable irrigation management, and inadequate drainage conditions. Salinity problems require sustainable management strategies, including identifying and further developing crop cultivation practices adapted to saline conditions, enhanced drainage systems, using salt-tolerant varieties/crops, and exchanging knowledge and transferring practical and adaptive solutions. Water is fundamental in agriculture; different sources of pollution such as sewage and industrial wastewater are discharged onto the drains. So, the water in this drain has very low quality, which in turn may cause hazards to soil and grown crops. It could be concluded that drains may be used for irrigation purposes under controlled precautions with good soil management, e.g., good tillage, deep plowing, land leveling, applying soil and water amendments, and finally a suitable cropping system.

Author Contributions: Conceptualization, H.M.A. and M.A.E.A.; methodology, H.M.A., M.A.E.A., A.M.S.K., M.S.M.E., K.A.A., T.H.K. and A.S.; software, H.M.A., M.A.E.A., A.M.S.K., M.S.M.E., K.A.A. and T.H.K.; validation, H.M.A., M.A.E.A., A.M.S.K., M.S.M.E., K.A.A., T.H.K. and A.S.; formal analysis, H.M.A., M.A.E.A., A.M.S.K., M.S.M.E., K.A.A. and T.H.K.; investigation, H.M.A., M.A.E.A., A.M.S.K., M.S.M.E., K.A.A., T.H.K. and A.S.; resources, H.M.A., M.A.E.A., A.M.S.K., M.S.M.E., K.A.A., T.H.K. and A.S.; data curation, H.M.A., M.A.E.A., A.M.S.K., M.S.M.E., K.A.A., T.H.K. and A.S.; writing—original draft preparation, H.M.A., M.A.E.A., A.M.S.K., M.S.M.E., K.A.A., T.H.K. and A.S.; writing—review and editing, H.M.A., M.A.E.A., A.M.S.K., M.S.M.E., K.A.A., T.H.K. and A.S.; visualization, H.M.A.; supervision, H.M.A. and M.A.E.A.; project administration, H.M.A., M.A.E.A., A.M.S.K., M.S.M.E., K.A.A. and T.H.K.; funding acquisition, H.M.A., M.A.E.A., A.M.S.K., M.S.M.E., K.A.A., T.H.K. and A.S. All authors have read and agreed to the published version of the manuscript.

Funding: This research received no external funding.

Data Availability Statement: Not applicable.

Acknowledgments: The manuscript presents a participation between the scientific institutions in two countries (Egypt and Italy), and in particular, the authors are grateful for their support in carrying out the work to: (1) National Authority for Remote Sensing and Space Sciences (NARSS), Cairo 11769, Egypt. (2) Soil, Water and Environment Research Institute (SWERI), Agricultural Research Centre (ARC), Giza 12112, Egypt. (3) SAFE-Università degli Studi della Basilicata.

Conflicts of Interest: The authors declare no conflict of interest.

References

1. Jiang, L.; Bao, A.; Jiapaer, G.; Liu, R.; Yuan, Y.; Yu, T. Monitoring Land Degradation and Assessing Its Drivers to Support Sustainable Development Goal 15.3 in Central Asia. *Sci. Total Environ.* **2022**, *807*, 150868. https://doi.org/10.1016/J.SCITOTENV.2021.150868.
2. Ziadat, F.M.; Zdruli, P.; Christiansen, S.; Caon, L.; Abdel Monem, M.; Fetsi, T.; An Overview of Land Degradation and Sustainable Land Management in the Near East and North Africa. *Sustain. Agric. Res.* **2022**, *11*, 11–24. https://doi.org/10.5539/sar.v11n1p11.
3. Kangalawe, R.Y. Land Degradation, Community Perceptions and Environmental Management Implications in the Drylands of Central Tanzania. In *Sustainable Development—Authoritative and Leading Edge Content for Environmental Management [Internet]*; Curkovic, S., Eds.; IntechOpen: London, UK, 2012. https://doi.org/10.5772/45897. Available online: https://www.intechopen.com/chapters/38100 (accessed on 27 June 2022).
4. Palmate, S.S.; Pandey, A.; Pandey, R.P.; Mishra, S.K. Assessing the Land Degradation and Greening Response to Changes in Hydro-climatic Variables Using a Conceptual Framework: A Case-study in Central India. *Land Degrad. Dev.* **2021**, *32*, 4132–4148.
5. Manorama, K.; Behera, S.K.; Suresh, K.; Prasad, M.V.; Mathur, R.K.; Harinarayana, P. Mulching and Technological Interventions Avoid Land Degradation in an Intensive Oil Palm (*Elaeis guineensis* Jacq.) Production System. *Land Degrad. Dev.* **2021**, *32*, 3785–3797.
6. Cerretelli, S.; Poggio, L.; Yakob, G.; Boke, S.; Habte, M.; Coull, M.; Peressotti, A.; Black, H.; Gimona, A. The Advantages and Limitations of Global Datasets to Assess Carbon Stocks as Proxy for Land Degradation in an Ethiopian Case Study. *Geoderma* **2021**, *399*, 115117. https://doi.org/10.1016/J.GEODERMA.2021.115117.

7. Rawat, L.S.; Maikhuri, R.K.; Bahuguna, Y.M.; Jugran, A.K.; Maletha, A.; Jha, N.K.; Phondani, P.C.; Dhyani, D.; Pharswan, D.S.; Chamoli, S. Rejuvenating Ecosystem Services through Reclaiming Degraded Land for Sustainable Societal Development: Implications for Conservation and Human Wellbeing. *Land Use Policy* **2022**, *112*, 105804. https://doi.org/10.1016/J.LANDUSEPOL.2021.105804.
8. Chotte, J.L.; Orr, B.J. Mitigating "Displaced" Land Degradation and the Risk of Spillover through the Decommoditization of Land Products. *Land Use Policy* **2021**, *109*, 105659. https://doi.org/10.1016/J.LANDUSEPOL.2021.105659.
9. Hossain, M.S. Present Scenario of Global Salt Affected Soils, Its Management and Importance of Salinity Research. *Int. Res. J. Biol. Sci.* **2019**, *1*, 1–3.
10. Mukhopadhyay, R.; Sarkar, B.; Jat, H.S.; Sharma, P.C.; Bolan, N.S. Soil Salinity under Climate Change: Challenges for Sustainable Agriculture and Food Security. *J. Environ. Manag.* **2021**, *280*, 111736. https://doi.org/10.1016/J.JENVMAN.2020.111736.
11. Sahab, S.; Suhani, I.; Srivastava, V.; Chauhan, P.S.; Singh, R.P.; Prasad, V. Potential Risk Assessment of Soil Salinity to Agroecosystem Sustainability: Current Status and Management Strategies. *Sci. Total Environ.* **2021**, *764*, 144164.
12. Ullah, A.; Bano, A.; Khan, N. Climate Change and Salinity Effects on Crops and Chemical Communication Between Plants and Plant Growth-Promoting Microorganisms Under Stress. *Front. Sustain. Food Syst.* **2021**, *5*, 618092. https://doi.org/10.3389/fsufs.2021.618092.
13. Giller, K.E.; Delaune, T.; Silva, J.V.; Descheemaeker, K.; Ven, G.V.; Schut, A.G.T.; Wijk, M.V.; Hammond, J.; Hochman, Z.; Taulya, G.; et al. The future of farming: Who will produce our food? *Food Secur.* **2021**, *13*, 1073–1099. https://doi.org/10.1007/s12571-021-01184-6.
14. Miao, Q.; Zhou, L.; Gonçalves, J.M.; Duarte, I.M.; Li, R.; Shi, H. Effects of Sand Addition to Heavy Saline-Alkali Soil on the Infiltration and Salt Leaching in Hetao Irrigation District, China. *Biol. Life Sci. Forum* **2021**, *3*, 33. https://doi.org/10.3390/IECAG2021-10156.
15. Yadav, M.S.; Yadav, P.P.S.; Yaduvanshi, M.; Verma, D.; Singh, A.N. Sustainability assessment of sodic land reclamation using remote sensing and GIS. *J. Indian Soc. Remote Sens.* **2010**, *38*, 269–278. https://doi.org/10.1007/s12524-010-0017-7.
16. Sayed, Y.A.; Fadl, M.E. Agricultural Sustainability Evaluation of the New Reclaimed Soils at Dairut Area, Assiut, Egypt using GIS Modeling. *Egypt. J. Remote Sens. Space Sci.* **2021**, *24*, 707–719.
17. Saeed, M.; Khafagi, O.; Bedair, R. Soil Quality Assessment for Wheat Cultivation in El–Menoufia Governorate, Nile Delta, Egypt. *J. Soil Sci. Agric. Eng.* **2018**, *9*, 693–698.
18. Sandeep, P.; Reddy, G.P.O.; Jegankumar, R.; Kumar, K.C.A. Modeling and Assessment of Land Degradation Vulnerability in Semi-Arid Ecosystem of Southern India Using Temporal Satellite Data, AHP and GIS. *Environ. Model. Assess.* **2021**, *26*, 143–154.
19. Pásztor, L. Advanced GIS and RS Applications for Soil and Land Degradation Assessment and Mapping. *ISPRS Int. J. Geo-Inf.* **2021**, *10*, 128.
20. Feng, R.; Wang, F.; Wang, K. Spatial-Temporal Patterns and Influencing Factors of Ecological Land Degradation-Restoration in Guangdong-Hong Kong-Macao Greater Bay Area. *Sci. Total Environ.* **2021**, *794*, 148671. https://doi.org/10.1016/J.SCITOTENV.2021.148671.
21. Vieira, R.M.D.S.P.; Tomasella, J.; Barbosa, A.A.; Polizel, S.P.; Ometto, J.P.H.B.; Santos, F.C.; Ferreira, Y.D.C.; de Toledo, P.M. Land Degradation Mapping in the MATOPIBA Region (Brazil) Using Remote Sensing Data and Decision-Tree Analysis. *Sci. Total Environ.* **2021**, *782*, 146900. https://doi.org/10.1016/J.SCITOTENV.2021.146900.
22. Farah, A.; Algouti, A.; Algouti, A.; Ifkirne, M.; Ezziyani, A. Mapping of Soil Degradation in Semi-Arid Environments in the Ouarzazate Basin in the South of the Central High Atlas, Morocco, Using Sentinel 2A Data. *Remote Sens. Appl. Soc. Environ.* **2021**, *23*, 100548. https://doi.org/10.1016/J.RSASE.2021.100548.
23. Higginbottom, T.P.; Symeonakis, E. Assessing Land Degradation and Desertification Using Vegetation Index Data: Current Frameworks and Future Directions. *Remote Sens.* **2014**, *6*, 9552–9575.
24. Gorji, T.; Sertel, E.; Tanik, A. Monitoring Soil Salinity via Remote Sensing Technology under Data Scarce Conditions: A Case Study from Turkey. *Ecol. Indic.* **2017**, *74*, 384–391. https://doi.org/10.1016/J.ECOLIND.2016.11.043.
25. Nouri, H.; Chavoshi Borujeni, S.; Alaghmand, S.; Anderson, S.J.; Sutton, P.C.; Parvazian, S.; Beecham, S. Soil Salinity Mapping of Urban Greenery Using Remote Sensing and Proximal Sensing Techniques; The Case of Veale Gardens within the Adelaide Parklands. *Sustainability* **2018**, *10*, 2826.
26. Mougenot, B.; Pouget, M.; Epema, G.F. Remote Sensing of Salt Affected Soils. *Remote Sens. Rev.* **1993**, *7*, 241–259. https://doi.org/10.1080/02757259309532180.
27. Reddy, G.P.O. Spatial Data Management, Analysis, and Modeling in GIS: Principles and Applications. In *Geospatial Technologies in Land Resources Mapping, Monitoring and Management*; Springer: New York, NY, USA, 2018; pp. 127–142.
28. Abuelgasim, A.; Ammad, R. Mapping Soil Salinity in Arid and Semi-Arid Regions Using Landsat 8 OLI Satellite Data. *Remote Sens. Appl. Soc. Environ.* **2019**, *13*, 415–425. https://doi.org/10.1016/J.RSASE.2018.12.010.
29. Alexakis, D.D.; Tapoglou, E.; Vozinaki, A.-E.K.; Tsanis, I.K. Integrated Use of Satellite Remote Sensing, Artificial Neural Networks, Field Spectroscopy, and GIS in Estimating Crucial Soil Parameters in Terms of Soil Erosion. *Remote Sens.* **2019**, *11*, 1106.
30. Prokop, P. Remote Sensing of Severely Degraded Land: Detection of Long-Term Land-Use Changes Using High-Resolution Satellite Images on the Meghalaya Plateau, Northeast India. *Remote Sens. Appl. Soc. Environ.* **2020**, *20*, 100432. https://doi.org/10.1016/J.RSASE.2020.100432.

31. Hassani, A.; Azapagic, A.; Shokri, N. Global predictions of primary soil salinization under changing climate in the 21st century. *Nat. Commun.* **2021**, *12*, 666. https://doi.org/10.1038/s41467-021-26907-3.
32. Hassani, A.; Azapagic, A.; Shokri, N. Predicting long-term dynamics of soil salinity and sodicity on a global scale. *Proc. Natl. Acad. Sci. USA* **2020**, *117*, 33017–33027. https://doi.org/10.1073/pnas.2013771117.
33. Richards, L.A. Diagnosis and Improvement of Saline and Alkali Soils. *LWW* **1954**, *78*, 154.
34. Mohanavelu, A.; Naganna, S.R.; Al-Ansari, N. Irrigation Induced Salinity and Sodicity Hazards on Soil and Groundwater: An Overview of Its Causes, Impacts and Mitigation Strategies. *Agriculture* **2021**, *11*, 983.
35. Wang, Z.; Zhang, F.; Zhang, X.; Chan, N.W.; te Kung, H.; Ariken, M.; Zhou, X.; Wang, Y. Regional Suitability Prediction of Soil Salinization Based on Remote-Sensing Derivatives and Optimal Spectral Index. *Sci. Total Environ.* **2021**, *775*, 145807. https://doi.org/10.1016/J.SCITOTENV.2021.145807.
36. Nabiollahi, K.; Taghizadeh-Mehrjardi, R.; Shahabi, A.; Heung, B.; Amirian-Chakan, A.; Davari, M.; Scholten, T. Assessing Agricultural Salt-Affected Land Using Digital Soil Mapping and Hybridized Random Forests. *Geoderma* **2021**, *385*, 114858. https://doi.org/10.1016/J.GEODERMA.2020.114858.
37. Elnaggar, A.A.; Noller, J.S. Application of Remote-Sensing Data and Decision-Tree Analysis to Mapping Salt-Affected Soils over Large Areas. *Remote Sens.* **2010**, *2*, 151–165.
38. Nguyen, K.-A.; Liou, Y.-A.; Tran, H.-P.; Hoang, P.-P.; Nguyen, T.-H. Soil Salinity Assessment by Using Near-Infrared Channel and Vegetation Soil Salinity Index Derived from Landsat 8 OLI Data: A Case Study in the Tra Vinh Province, Mekong Delta, Vietnam. *Prog. Earth Planet. Sci.* **2020**, *7*, 1–16.
39. Jiang, X.; Duan, H.; Liao, J.; Guo, P.; Huang, C.; Xue, X. Estimation of Soil Salinization by Machine Learning Algorithms in Different Arid Regions of Northwest China. *Remote Sens.* **2022**, *14*, 347. https://doi.org/10.3390/rs14020347.
40. Scudiero, E.; Skaggs, T.H.; Corwin, D.L. Regional-Scale Soil Salinity Assessment Using Landsat ETM+ Canopy Reflectance. *Remote Sens. Environ.* **2015**, *169*, 335–343.
41. Nguyen, A.K.; Liou, Y.-A.; Li, M.-H.; Tran, T.A. Zoning Eco-Environmental Vulnerability for Environmental Management and Protection. *Ecol. Indic.* **2016**, *69*, 100–117.
42. Liou, Y.-A.; Nguyen, A.K.; Li, M.-H. Assessing Spatiotemporal Eco-Environmental Vulnerability by Landsat Data. *Ecol. Indic.* **2017**, *80*, 52–65.
43. AL-Khakani, E.T.; Al-Janabi, W.F.; Sa'ad, R.Y.; Al-Kazaali, H.M. Using Landsat 8 OLI Data to Predict and Mapping Soil Salinity for Part of An-Najaf Governorate. *Ecol. Environ. Conserv.* **2018**, *24*, 572–578.
44. Essahlaoui, A.; Teodoro, A.C.; Mohajane, M. Modeling and Mapping of Soil Salinity in Tafilalet Plain (Morocco). *Arab. J. Geosci.* **2019**, *12*, 1–7.
45. El Baroudy. A.A. Monitoring land degradation using remote sensing and GIS techniques in an area of the middle Nile Delta, Egypt. *Catena* **2011**, *87*, 201–208. https://doi.org/10.1016/j.catena.2011.05.023.
46. Mohamed, E.S.; Belal, A.; Saleh, A. Assessment of Land Degradation East of the Nile Delta, Egypt Using Remote Sensing and GIS Techniques. *Arab. J. Geosci.* **2013**, *6*, 2843–2853.
47. Arnous, M.O.; Green, D.R. Monitoring and Assessing Waterlogged and Salt-Affected Areas in the Eastern Nile Delta Region, Egypt, Using Remotely Sensed Multi-Temporal Data and GIS. *J. Coast. Conserv.* **2015**, *19*, 369–391.
48. El Baroudy, A.A. Mapping and Evaluating Land Suitability Using a GIS-Based Model. *Catena* **2016**, *140*, 96–104.
49. Ali, R.R.; Saber, M.; Nizinski, J.J.; Montoroi, J.-P.; Zaghloul, A.M. Land Surface Analysis of Salt Affected Soils Using DEM and GIS. *Eur. J. Sci. Res.* **2016**, *138*, 197–202.
50. Elbasiouny, H.; Elbehiry, F.; Abowaly, M. Soil Quality Indices; Special Focus on Salt-Affected Soil: Review and Case Study in Northern Egypt. *Environ. Biodivers. Soil Secur.* **2017**, *1*, 85–100.
51. Yossif, M.H.T. Change Detection of Land Cover and Salt Affected Soils at Siwa Oasis, Egypt. *Alex. Sci. Exch. J.* **2017**, *38*, 446–462.
52. Abou Samra, R.M.; Ali, R.R. The Development of an Overlay Model to Predict Soil Salinity Risks by Using Remote Sensing and GIS Techniques: A Case Study in Soils around Idku Lake, Egypt. *Environ. Monit. Assess.* **2018**, *190*, 1–16.
53. AbdelRahman, M.A.E.; Metwaly, M.M.; Shalaby, A. Quantitative Assessment of Soil Saline Degradation Using Remote Sensing Indices in Siwa Oasis. Remote Sens. *Appl. Soc. Environ.* **2019**, *13*, 53–60.
54. AbdelRahman, M.A.E.; Natarajan, A.; Hegde, R.; Prakash, S.S. Assessment of Land Degradation Using Comprehensive Geostatistical Approach and Remote Sensing Data in GIS-Model Builder. *Egypt. J. Remote Sens. Space Sci.* **2019**, *22*, 323–334. https://doi.org/10.1016/J.EJRS.2018.03.002.
55. El Baroudy, A.A.; Moghanm, F.S. Combined use of remote sensing and GIS for degradation risk assessment in some soils of the Northern Nile Delta, Egypt. *Egypt. J. Remote Sens. Space Sci.* **2014**, *17*, 77–85. https://doi.org/10.1016/j.ejrs.2014.01.001.
56. Shokr, M.S.; Abdellatif, M.; El Baroudy, A.A.; Elnashar, A.; Ali, E.F.; Belal, A.A.; Attia, W.; Ahmed, M.; Aldosari, A.A.; Szantoi, Z. Development of a Spatial Model for Soil Quality Assessment under Arid and Semi-Arid Conditions. *Sustainability* **2021**, *13*, 2893.
57. Gabriel, J.L.; Vanclooster, M.; Quemada, M. Integrating Water, Nitrogen, and Salinity in Sustainable Irrigated Systems: Cover Crops versus Fallow. *J. Irrig. Drain. Eng.* **2014**, *140*, A4014002.
58. Zayed, A.M.A.; Al-Toukhy, A.A.; El-Tapey, H.M.A. Pedological features of some Western Delta soils, Egypt and their relationships with different taxonomic systems. *Middle East J. Agric. Res.* **2021**, *10*, 852–865. https://doi.org/10.36632/mejar/2021.10.3.58.

59. El-Ramady, H.; Abowaly, M.; Elbehiry, F.; Omara, A.E.; Elsakhawy, T.; Mohamed, E.S.; Belal, A.; Elbasiouny, H.; Fawzy, Z.F. Stressful Environments and Sustainable Soil Management: A Case Study of Kafr El-Sheikh, Egypt. *Environ. Biodivers. Soil Secur.* **2019**, *3*, 193–213.
60. Mahdy, E.E.; Mahrous, H.; Sayed, M.A.; Housein, M.G. Salinity indices and path analysis in Egyptian long-staple cotton cultivars. *SVU-Int. J. Agric. Sci.* **2021**, *13*, 105–118. https://doi.org/10.21608/SVUIJAS.2021.94700.1140.
61. Shaddad, S.M.; Hendawi, M.Y. Site-Specific Leaching Map of a Salt Affected Soil in Egypt. *Biomed. J. Sci. Tech. Res.* **2018**, *2*, 2768–2773.
62. Shahid, S.A.; Zaman, M.; Heng, L. Introduction to Soil Salinity, Sodicity and Diagnostics Techniques. In *Guideline for Salinity Assessment, Mitigation and Adaptation Using Nuclear and Related Techniques*; Springer: Cham, Switzerland, 2018. https://doi.org/10.1007/978-3-319-96190-3_1.
63. Li, J.; Pu, L.; Zhu, M.; Zhang, R. The Present Situation and Hot Issues in the Salt-Affected Soil Research. *Acta Geogr. Sin* **2012**, *67*, 1233–1245.
64. Zhang, Y.; Li, X.; Šimůnek, J.; Shi, H.; Chen, N.; Hu, Q.; Tian, T. Evaluating Soil Salt Dynamics in a Field Drip-Irrigated with Brackish Water and Leached with Freshwater during Different Crop Growth Stages. *Agric. Water Manag.* **2021**, *244*, 106601.
65. Gupta, M.; Srivastava, P.K.; NIRANJAN, A.; TEWARI, S.K. Use of a Bioaugmented Organic Soil Amendment in Combination with Gypsum for Withania Somnifera Growth on Sodic Soil. *Pedosphere* **2016**, *26*, 299–309.
66. Alcívar, M.; Zurita-Silva, A.; Sandoval, M.; Muñoz, C.; Schoebitz, M. Reclamation of Saline–Sodic Soils with Combined Amendments: Impact on Quinoa Performance and Biological Soil Quality. *Sustainability* **2018**, *10*, 3083.
67. Kost, D.; Ladwig, K.J.; Chen, L.; DeSutter, T.M.; Espinoza, L.; Norton, L.D.; Smeal, D.; Torbert, H.A.; Watts, D.B.; Wolkowski, R.P. Meta-Analysis of Gypsum Effects on Crop Yields and Chemistry of Soils, Plant Tissues, and Vadose Water at Various Research Sites in the USA. *J. Environ. Qual.* **2018**, *47*, 1284–1292.
68. Presley, D.; He, Y.; Tomlinson, P. Soil Health and Yields on Non-Sodic Soils Amended with Flue Gas Desulfurization Gypsum. Crop. *Forage Turfgrass Manag.* **2018**, *4*, 1–6.
69. Safdar, H.; Amin, A.; Shafiq, Y.; Ali, A.; Yasin, R.; Shoukat, A.; Hussan, M.U.; Sarwar, M.I. A Review: Impact of Salinity on Plant Growth. *Nat. Sci.* **2019**, *17*, 34–40.
70. Fontoura, S.M.V.; de Castro Pias, O.H.; Tiecher, T.; Cherubin, M.R.; de Moraes, R.P.; Bayer, C. Effect of Gypsum Rates and Lime with Different Reactivity on Soil Acidity and Crop Grain Yields in a Subtropical Oxisol under No-Tillage. *Soil Tillage Res.* **2019**, *193*, 27–41.
71. Aboelsoud, H.; Engel, B.; Gad, K. Effect of Planting Methods and Gypsum Application on Yield and Water Productivity of Wheat under Salinity Conditions in North Nile Delta. *Agronomy* **2020**, *10*, 853.
72. Zhang, Y.; Jingsong, Y.; Rongjiang, Y.A.O.; Xiangping, W.; Wenping, X.I.E. Short-Term Effects of Biochar and Gypsum on Soil Hydraulic Properties and Sodicity in a Saline-Alkali Soil. *Pedosphere* **2020**, *30*, 694–702.
73. El-Hady, A.; Abdrabelnabi, M.; Abdelaty, E.F. GIS—Comprehensive Analytical Approach for Soil Use by Linking Crop Soil Suitability to Soil Management and Reclamation. *Alex. Sci. Exch. J.* **2019**, *40*, 60–81.
74. Kotb, T.H.S.; Watanabe, T.; Ogino, Y.; Tanji, K.K. Soil salinization in the Nile Delta and related policy issues in Egypt. *Agric. Water Manag.* **2000**, *43*, 239–261.
75. Mohamed, E.; Belal, A.-A.; Ali, R.R.; Saleh, A.; Hendawy, E.A. Land Degradation. In *The Soils of Egypt*; Springer: Cham, Switzerland, 2019; pp. 159–174.
76. Aitta, A.; El-Ramady, H.; Alshaal, T.; El-Henawy, A.; Shams, M.; Talha, N.; Elbehiry, F.; Brevik, E.C. Seasonal and Spatial Distribution of Soil Trace Elements around Kitchener Drain in the Northern Nile Delta, Egypt. *Agriculture* **2019**, *9*, 152. https://doi.org/10.3390/agriculture9070152.
77. Abd-Elwahed, M.S. Influence of long-term wastewater irrigation on soil quality and its spatial distribution. *Ann. Agric. Sci.* **2018**, *63*, 191–199.
78. El-Alfy, M.A.; El-Amier, Y.A.; Abd El-Hamid, H.T. Soil quality and health risk assessment of heavy metals in agricultural areas irrigated with wastewater from Kitchener Drain, Nile Delta, Egypt. *J. Sci. Agric.* **2017**, *1*, 158–170.
79. Eid, E.M.; Galal, T.M.; Sewelam, N.A.; Talha, N.I.; Abdallah, S.M. Phytoremediation of heavy metals by four aquatic macrophytes and their potential use as contamination indicators: A comparative assessment. *Environ. Sci. Pollut. Res.* **2020**, *27*, 12138–12151. https://doi.org/10.1007/s11356-020-07839-9.
80. AbdelRahman, M.A.E.; Shalaby, A.; Aboelsoud, M.H.; Moghanm, F.S. GIS Spatial Model Based for Determining Actual Land Degradation Status in Kafr El-Sheikh Governorate, North Nile Delta. *Model. Earth Syst. Environ.* **2018**, *4*, 359–372.
81. AbdelRahman, M.A.E.; Afifi, A.A.; Scopa, A. A Time Series Investigation to Assess Climate Change and Anthropogenic Impacts on Quantitative Land Degradation in the North Delta, Egypt. *ISPRS Int. J. Geo-Inf.* **2022**, *11*, 30.
82. *Conoco Geologic Map of Egypt. Egyptian General Authority for Petroleum (UNESCO Joint Map Project), 20 Sheets, Scale 1:50,000*; Conoco Geologic Map of Egypt: Cairo, Egypt, 1987.
83. Said, R. *The River Nile Geology and Hydrology and Utilization by Rushdi Said*; Pergman Press: Oxford, UK, 1993.
84. MWRI. *Water Resources Plan for Kafr El-Sheikh Governorate, The National Water Resources Plan Project*; MWRI: Pittsburgh, PA, USA, 2016.
85. Alkhawaga, A.; Zeidan, B.; Elshemy, M. Climate change impacts on water security elements of Kafr El-Sheikh governorate, Egypt. *Agric. Water Manag.* **2022**, *259*, 107217. https://doi.org/10.1016/j.agwat.2021.107217.
86. Ali, H.M.; EL-Mahrouk, E.M.; Hassan, F.A.; EL-Tarawy, M.A. Usage of sewage effluent in irrigation of some woody tree seedlings. Part 3: *Swietenia mahagoni* (L.) Jacq. *Saudi J. Biol. Sci.* **2011**, *18*, 201–207.

87. Page, A.L.; Miller, R.H.; Keeney, D.R. *Methods of Soil Analysis, Part 2—Chemical and Microbiological Properties*, 2nd ed.; American Society of Agronomy, Inc. Soil Science Society of America, Inc. Publishers: Madison, WI, USA, 1982.
88. Nelson, D.W.; Sommers, L. Total Carbon, Organic Carbon, and Organic Matter. *Methods Soil Anal. Part 2 Chem. Microbiol. Prop.* **1983**, *9*, 539–579.
89. Cottenie, A.; Verloo, M.; Kiekens, L.; Velghe, G.; Camerlynck, R. *Chemical Analysis of Plants and Soils*; Laboratory Agrochemicals State University: Gent, Belgium, 1982; p. 63.
90. Rhoades, J.D. Drainage for Salinity Control. *Drain. Agric.* **1974**, *17*, 433–461.
91. ESRI. *ArcGIS Desktop Spatial Analyst Extension: Release 10.1*; Enviromental Systems Research Institute: Redlands, CA, USA, 2012.
92. Dehni, A.; Lounis, M. Remote Sensing Techniques for Salt Affected Soil Mapping: Application to the Oran Region of Algeria. *Procedia Eng.* **2012**, *33*, 188–198.
93. AbdelRahman, M.A.E.; Afifi, A.A.; D'Antonio, P.; Gabr, S.S.; Scopa, A. Detecting and Mapping Salt-Affected Soil with Arid Integrated Indices in Feature Space using Multi-Temporal Landsat Imagery. *Remote Sens.* **2022**, *14*, 2599. https://doi.org/10.3390/rs14112599.
94. Khan, N.M.; Rastoskuev, V.V.; Sato, Y.; Shiozawa, S. Assessment of hydrosaline land degradation by using a simple approach of remote sensing indicators. *Agric. Water Manag.* **2005**, *77*, 96–109.
95. Alhammadi, M.S.; Glenn, E.P. Detecting Date Palm Trees Health and Vegetation Greenness Change on the Eastern Coast of the United Arab Emirates Using SAVI. *Int. J. Remote Sens.* **2008**, *29*, 1745–1765.
96. Nicolas, H.; Walter, C. Detecting Salinity Hazards within a Semiarid Context by Means of Combining Soil and Remote-Sensing Data. *Geoderma* **2006**, *134*, 217–230.
97. Bannari, A.; Guedon, A.M.; El-Harti, A.; Cherkaoui, F.Z.; El-Ghmari, A. Characterization of Slightly and Moderately Saline and Sodic Soils in Irrigated Agricultural Land Using Simulated Data of Advanced Land Imaging (EO-1) Sensor. *Commun. Soil Sci. Plant Anal.* **2008**, *39*, 2795–2811.
98. Khan, S.; Abbas, A. *Using Remote Sensing Techniques for Appraisal of Irrigated Soil Salinity*; Integrated Systems for Sustainability MODSIM07; Modelling and Simulation Society of Australia and New Zealand: Christchurch, New Zealand, 2007; pp. 2632–2638.
99. Kaufman, Y.J.; Wald, A.E.; Remer, L.-A.; Gao, B.C.; Li, R.R.; Flynn, L. The MODIS 2.1-mm channel-correlation with visible reflectance for use in remote sensing of aerosol. *IEEE Trans. Geosci. Remote Sens.* **1997**, *35*, 1286–1298.
100. Felde, G.W.; Anderson, G.P.; Adler-Golden, S.M.; Matthew, M.W.; Berk, A. Analysis of Hyperion data with the FLAASH atmospheric correction algorithm. In Proceedings of the Algorithms and Technologies for Multispectral, Hyperspectral, and Ultraspectral Imagery IX, SPIE Aerosense Conference, Orlando, FL, USA, 21–25 April 2003.
101. Zanter, K. *Landsat 8 (L8) Data Users Handbook, LSDS-1574, Version 2.0, March 29 2016*; Department of the Interior U.S. Geological Survey, EROS: Sioux Falls, SD, USA, 2016.
102. Allbed, A.; Kumar, L.; Sinha, P. Mapping and Modelling Spatial Variation in Soil Salinity in the Al Hassa Oasis Based on Remote Sensing Indicators and Regression Techniques. *Remote Sens.* **2014**, *6*, 1137–1157.
103. Asfaw, E.; Suryabhagavan, K.V.; Argaw, M. Soil Salinity Modeling and Mapping Using Remote Sensing and GIS: The Case of Wonji Sugar Cane Irrigation Farm, Ethiopia. *J. Saudi Soc. Agric. Sci.* **2018**, *17*, 250–258. https://doi.org/10.1016/J.JSSAS.2016.05.003.
104. Elhag, M. Evaluation of Different Soil Salinity Mapping Using Remote Sensing Techniques in Arid Ecosystems, Saudi Arabia. *J. Sens.* **2016**, *2016*, 1–8.
105. Enar, K.A.; El Baroudy, A.A.; Shokr, M.S. Assessment and mapping land degradation in some areas of North Nile Delta, using new techniques. *Menoufia J. Soil Sci.* **2021**, *6*, 265–274.
106. Antar, S.A.; El-Sanat, G.M.A.; Khafagy, H.A. Improving Heavy Clay Salt Affected Soil and Its Production Using Some Amendments Application In North Delta. *J. Soil Sci. Agric. Eng.* **2014**, *5*, 1717–1730.
107. Kassem, H.S.; Bello, A.R.S.; Alotaibi, B.M.; Aldosri, F.O.; Straquadine, G.S. Climate Change Adaptation in the Delta Nile Region of Egypt: Implications for Agricultural Extension. *Sustainability* **2019**, *11*, 685. https://doi.org/10.3390/su11030685.
108. Fawaz, M.M.; Soliman, S.A. The potential scenarios of the impacts of climate change on Egyptian resources and agricultural plant production. *Open J. Appl. Sci.* **2016**, *6*, 270–286.
109. Eid, H.M.; El-Marsafawy, S.M.; Ouda, S.A. *Assessing the Economic Impacts of Climate Change on Agriculture in Egypt: A Ricardian Approach*; Policy Research Working Paper 4293; World Bank: Washington, DC, USA, 2007.
110. Kheir, M.S.; El Baroudy, A.; Aiad, M.A.; Zoghdan, M.G.; Abd El-Aziz, M.A.; Ali, M.G.; Fullen, M.A. Impacts of rising temperature, carbon dioxide concentration and sea level on wheat production in North Nile Delta. *Sci. Total Environ.* **2019**, *651*, 3161–3173.
111. El-Amier, Y.A.; Zahran, M.A.; Gebreil, A.S.; Abd El-Salam, E.H. Anthropogenic activities and their impact on the environmental status of Kitchener drain, Nile Delta, Egypt. *J. Environ. Sci.* **2017**, *46*, 251–262.
112. Nehela, Y.; Mazrou, Y.S.A.; Alshaal, T.; Rady, A.M.S.; El-Sherif, A.M.A.; Omara, A.E.-D.; Abd El-Monem, A.M.; Hafez, E.M. The Integrated Amendment of Sodic-Saline Soils Using Biochar and Plant Growth-Promoting Rhizobacteria Enhances Maize (*Zea mays* L.) Resilience to Water Salinity. *Plants* **2021**, *10*, 1960. https://doi.org/10.3390/plants10091960.
113. Abou El Hassan, W.H. Impact Assessment Of Long Term Climate Change On Reference Evapotranspiration And Water Management In North Delta. *J. Soil Sci. Agric. Eng.* **2011**, *2*, 623–634.
114. Sun, B.; Li, Z.; Gao, Z.; Guo, Z.; Wang, B.; Hu, X.; Bai, L. Grassland Degradation and Restoration Monitoring and Driving Forces Analysis Based on Long Time-Series Remote Sensing Data in Xilin Gol League. *Acta Ecol. Sin.* **2017**, *37*, 219–228.

115. Scudiero, E.; Skaggs, T.H.; Corwin, D.L. Regional Scale Soil Salinity Evaluation Using Landsat 7, Western San Joaquin Valley, California, USA. *Geoderma Reg.* **2014**, *2*, 82–90.
116. CHU, L.; KANG, Y.; WAN, S. Effect of Different Water Application Intensity and Irrigation Amount Treatments of Microirrigation on Soil-Leaching Coastal Saline Soils of North China. *J. Integr. Agric.* **2016**, *15*, 2123–2131.
117. Machado, R.M.A.; Serralheiro, R.P. Soil Salinity: Effect on Vegetable Crop Growth. Management Practices to Prevent and Mitigate Soil Salinization. *Horticulturae* **2017**, *3*, 30.
118. Roy, S.; Chowdhury, N. Effects of leaching on the reclamation of saline soils as affected by different organic and inorganic amendments. *J. Environ. Sci. Sustain. Dev.* **2020**, *3*, 7.
119. Wang, N.; Xue, J.; Peng, J.; Biswas, A.; He, Y.; Shi, Z. Integrating Remote Sensing and Landscape Characteristics to Estimate Soil Salinity Using Machine Learning Methods: A Case Study from Southern Xinjiang, China. *Remote Sens.* 2020, *12*, 4118, doi:10.3390/rs12244118.
120. El-Saka, M.S. Evaluation of Drainage Water Quality of El Hoks Drain at North Nile Delta, Kafr El-Sheihk Governorate, Egypt. *J. Soil Sci. Agric. Eng.* **2020**, *11*, 291–297.
121. Dong, R.; Na, X. Quantitative Retrieval of Soil Salinity Using Landsat 8 OLI Imagery. *Appl. Sci.* **2021**, *11*, 11145. https://doi.org/10.3390/app112311145.
122. Wang, J.; Wang, W.; Hu, Y.; Tian, S.; Liu, D. Soil Moisture and Salinity Inversion Based on New Remote Sensing Index and Neural Network at a Salina-Alkaline Wetland. *Water* **2021**, *13*, 2762. https://doi.org/10.3390/w13192762.
123. Barrett-Lennard, E.G.; Munir, R.; Mulvany, D.; Williamson, L.; Riethmuller, G.; Wesley, C.; Hall, D. Micro-Water Harvesting and Soil Amendment Increase Grain Yields of Barley on a Heavy-Textured Alkaline Sodic Soil in a Rainfed Mediterranean Environment. *Agronomy* **2021**, *11*, 713. https://doi.org/10.3390/agronomy11040713.
124. .Naimi, S.; Ayoubi, S.; Zeraatpisheh, M.; Dematte, J.A.M. Ground Observations and Environmental Covariates Integration for Mapping of Soil Salinity: A Machine Learning-Based Approach. *Remote Sens.* **2021**, *13*, 4825.